

PROCEEDINGS OF SPIE

[SPIDigitalLibrary.org/conference-proceedings-of-spie](https://spiedigitallibrary.org/conference-proceedings-of-spie)

Influence of sidewall perturbations of CD-SEM line roughness metrology

Benjamin D. Bunday, Chris A. Mack, Sergei Borisov, Vera Sinitsina

Benjamin D. Bunday, Chris A. Mack, Sergei Borisov, Vera Sinitsina,
"Influence of sidewall perturbations of CD-SEM line roughness metrology,"
Proc. SPIE 10959, Metrology, Inspection, and Process Control for
Microlithography XXXIII, 109591Z (26 March 2019); doi: 10.1117/12.2519312

SPIE.

Event: SPIE Advanced Lithography, 2019, San Jose, California, United States

Influence of Sidewall Perturbations on CD-SEM Line Roughness Metrology

Benjamin D. Bunday^a, Chris A. Mack^b, Sergei Borisov^c, Vera Sinitsina^c

^aaBeam Technologies, Inc., Albany, NY, 12303, USA, E-mail: bb@abeamtech.com

^bFractilia, 1605 Watchhill Rd, Austin, TX 78703, E-mail: chris.mack@fractilia.com

^caBeam Technologies, Inc., Moscow, Russia

ABSTRACT

Microscopically, a rough edge can be considered as a set of exclusions (i.e., bumps) and inclusions (i.e., divots) along a sidewall. These local perturbations along the sidewall can be thought of as the most basic building blocks of the geometry of rough edges. However, these two structural geometries image differently under critical dimension scanning electron microscopes (CD-SEM), and also when scanned from different directions. An understanding of these imaging differences should be important to improving roughness measurement accuracy. In this work, images from using Monte Carlo and analytical simulations of different sizes of exclusions and inclusions on flat edges are used to better understand the effects of the local microgeometry of the edge, and also how various SEM algorithm choices, parameters, beam size/shape, charging, scan direction, and pixel size/scanning scheme influence SEM line edge uncertainties for such features. Furthermore, how these errors interact with roughness power spectral density (PSD) metrics will be explored, imparting knowledge for optimizing roughness PSD measurement with minimized error.

Keywords: CD-SEM, LER, LWR, roughness, linescan, charging, Monte Carlo, simulation

INTRODUCTION

As geometries continue to shrink in the integrated circuit (IC) industry, line-edge roughness (LER) continues to be a key limit to robust fabrication of advanced features. Low error measurement of roughness is of paramount importance in learning to control such edge imperfections. In this work we will show a simulation study [1,2] demonstrating how basic sidewall features are convolved with the blur of a scanning electron microscope (SEM) beam and how to evaluate the effective edge blur. We will then use effective blur measurements to quantify the effects of charging on roughness measurement, a key component that usually is neglected due to extreme difficulty in isolating the phenomenon experimentally, while also being time-prohibitive to explore through simulations. Charging has, ever since CD-SEMs began to be used, been typically and broadly observed to cause asymmetrical effects to critical dimension (CD) measurements through the asymmetrical waveform. However, such asymmetrical effects to roughness measurements have not been quantitatively studied for deeper understanding. Here we will attempt to estimate the effects on roughness measurement, particularly to understand the effect on power spectral density (PSD) metrics [3-7].

As with any scanning probe microscopy, the probe size and shape are key considerations. In CD-SEMs, this probe is an electron beam which has a non-zero spot size when projected onto the sample surface, with an approximately Gaussian intensity cross-section. Effective probe size for CD-SEMs also includes a scattering area component due to the interaction volume of the electrons within the sample, also of interest for study. This effective probe size acts as an imaging filter, the SEM's "image transfer function" which convolves with the sample features to produce the SEM image. As with many complex systems with many unknowable inputs, a Gaussian distribution is a good choice to describe the net effect of this SEM blurring, such that convoluting the sample's edge geometry with a Gaussian gives an approximation of the image. See Figure 1 for an illustration.

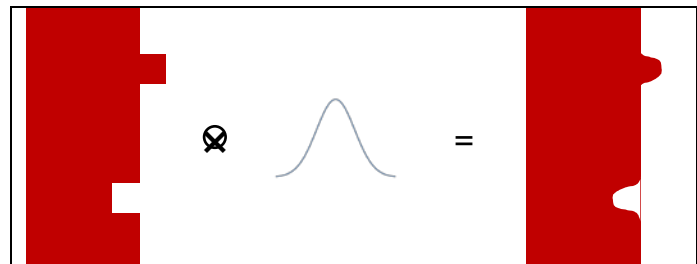


Figure 1: Illustration showing how ideal sample edge shape convolves with a Gaussian blur to achieve the typically observed curved form factor for the exclusions and inclusions.

In a previous work, one of the authors has quantitatively demonstrated that such SEM blurring reduces the high frequency PSD of a rough edge. [8] See Figure 2 for an illustration. Here, η is defined as the full width at half maximum (FWHM) of the Gaussian measurement blur; if the green $\eta = 0$ curve is the PSD for the defined shape with zero blur, and if Δy is the pixel size along the line length, the PSD for imaging that same edge with blur of $\eta = \Delta y$ (i.e. one pixel of blur) and $\eta = 2\Delta y$ (two pixels of blur) are shown with blue and purple curves respectively, and through this family of curves, it is observed that the high frequency PSD is significantly suppressed as the blur increases.

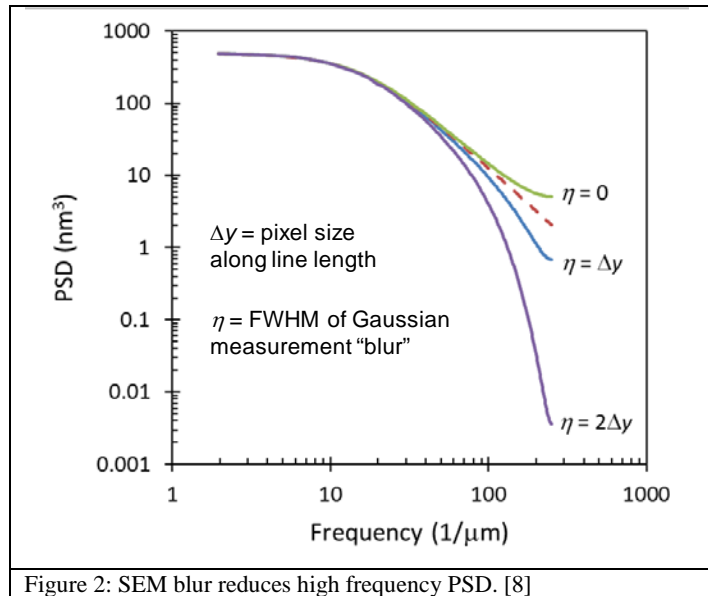


Figure 2: SEM blur reduces high frequency PSD. [8]

Below, Figure 3 shows simulated PSD with typical noise. The top graph includes no SEM blurring, while the bottom graph shows four pixels worth of blurring influencing the PSD. Note that the added blur noticeably decreases the PSD where spatial frequency is $> 0.08 \text{ nm}^{-1}$. This has the effect of increasing the measured roughness exponent (it changed from 0.81 to 0.87 due to the added blur), while also reducing the area under the PSD curve, which means the measured LER will also slightly decrease since LER is the integral under the PSD.

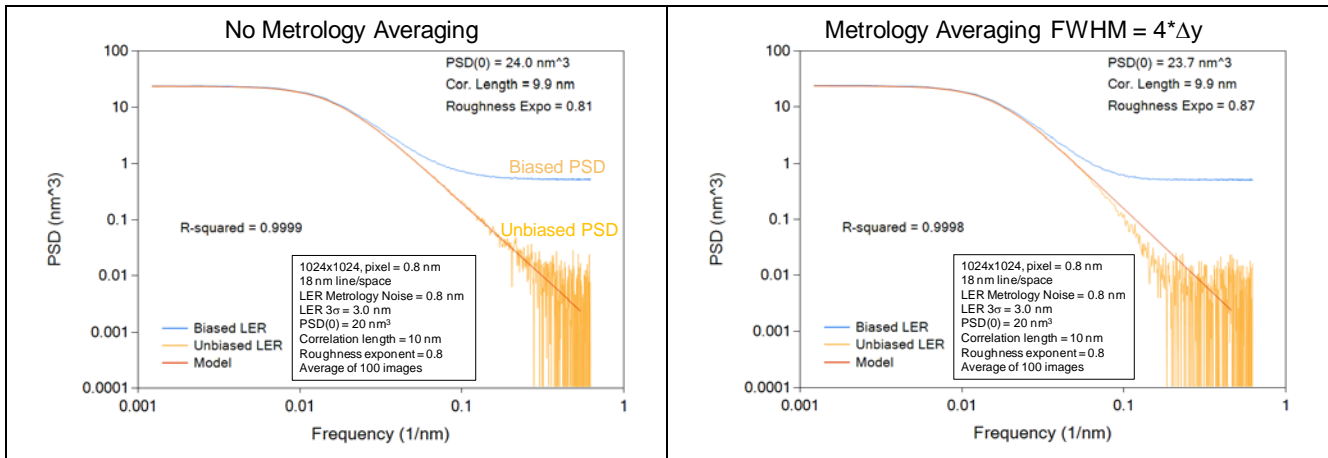


Figure 3: Simulated PSD with typical noise (using Fractilia's MetroLER software). Top: No SEM blur added. Bottom: Four pixels of SEM blur added (FWHM), resulting in the PSD being depressed at higher spatial frequencies.

SIMULATION STUDY OVERVIEW

To perform the study outlined above, a design of experiments (DOE) of different exclusions (tabs) and inclusions (divots) of varied designed dimensions was defined. These tab/divot features are located on the sidewall of a 100 nm wide photoresist line (called the carrier line) of vertical profile and 50 nm height on a Si substrate. The tabs are added as same photoresist material and same height as the carrier line, and the inclusions as vacuum cutouts from the sidewall of the carrier line. Each of the features is spaced exactly 20 nm apart (center-to-center) along the edge so electron trajectories from one sidewall feature are isolated enough that interactions with adjacent features are avoided. The DOE is defined with eight different widths of the features (defined as the distance along the sidewall in the y direction): 0.25 nm, 0.5 nm, 0.75 nm, 1.0 nm, 1.25 nm, 1.5 nm, 2.0 nm and 3.0 nm. For each of those feature widths, three different

versions with varying amplitudes of the feature are also defined, so each of the widths has a version with 0.5 nm, 1.0 nm and 1.5 nm amplitude, defined as the distance from the edge of the carrier line, in the x direction. These sidewall features are designed on both the left and right sidewalls of the carrier line.

These features were input into the simulation software, and Figure 4 illustrates the sample view from the simulation software GUI. Note the realized features are ideal boxes with all right angles, perfect corners and perfectly smooth sides, or in other words, “cartoon perfect”.

Two types of simulators were used to generate the simulated images for this work. They are discussed below.

Monte Carlo (MC) simulators are the most accurate simulators available, as they use all the known interaction and scattering functions from first principles to calculate realistic trajectories of each and every electron, including generation of backscattered and secondary electrons and the charging imbalances resulting from electron generation and absorption by the sample, and buildup/conduction/dissipation of the imbalanced charges within the sample. However, while such MC calculations are the most accurate possible with current technology, calculations are time consuming, usually hours per image, and when including charging effects, days per image. [1][2]

An alternative is to use a Fast Analytical simulator.[9][10] These include analytical models which closely match the MC outputs, basically as an extrapolation of the general waveform behaviors observed from MC results. Charging effects can also be included in such calculations. While these FA simulators are close to accurate to MC results, there usually are some slight differences from the results to MC simulations, so the results are close but not perfect. However, FA simulators have a different important advantage—speed. Even including charging effects, the same images that take days with MC simulations take only a minute or two with FA simulations, allowing larger charging studies to be performed economically.

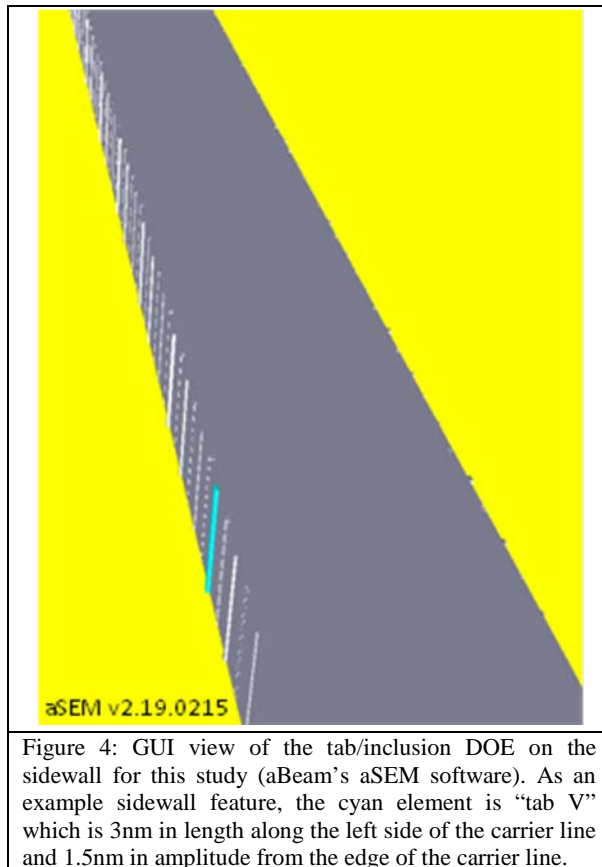


Figure 4: GUI view of the tab/inclusion DOE on the sidewall for this study (aBeam's aSEM software). As an example sidewall feature, the cyan element is “tab V” which is 3nm in length along the left side of the carrier line and 1.5nm in amplitude from the edge of the carrier line.

In this study, a simulator of each type was available. As a bonus, the simulators are from the same manufacturer and have almost identical GUI-based definition of the features, materials and simulation parameters, so that it was simple to adapt the sample designs and simulation parameters to both in a consistent manner. Also, outputs were in same format which allowed analysis without any further adaptation between the two data sets.

For Monte Carlo simulations, CHARIOT v5.18.1127 by aBeam was used, with aSEM v2.19.0215 by aBeam used for Fast Analytical simulations. The initial plan for this work was to use all MC simulations, but each of the 48 required images with charging would have taken several days (48 due to 8 widths x 3 amplitudes x 2 sidewalls) and available computation resources dedicated this work were not enough for this to be practical. So instead, a validation exercise was performed to match the waveforms of the FA results to the MC results. The case used was the waveform including charging effects at each edge of the feature. Figure 5 shows the waveform comparison at the left edge, with example images from each simulator type. For this validation, the MC waveform was simulated using 500 V beam with 10 pA probe current, 20 ns integration time/pixel/frame with 50 frames. The beam's spot was defined as a 1.2 nm FWHM Gaussian-profile, which has been observed to be similar spot size to contemporary top-of-the-line CD-SEMs.

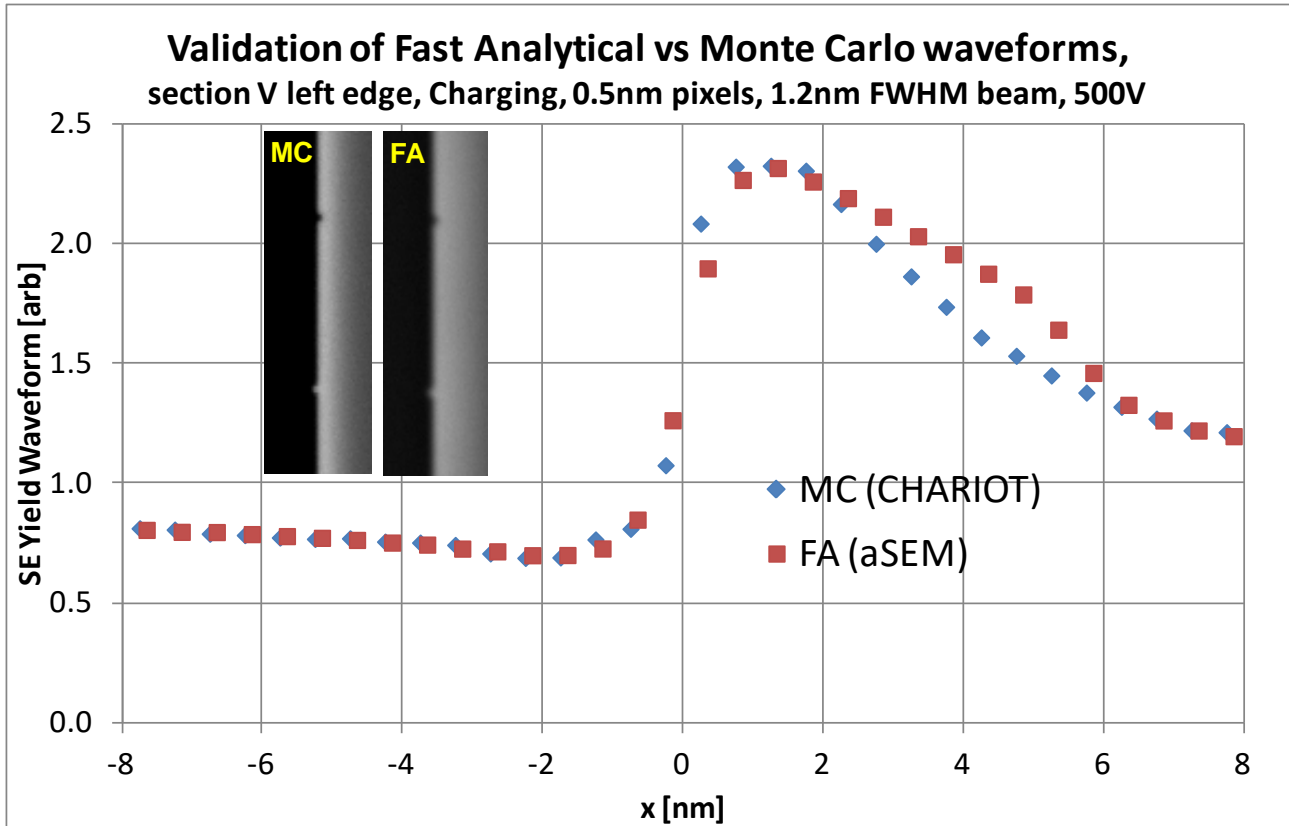


Figure 5: Validation of waveform matching between MC and FA solutions on left edge of the carrier line. Similar results were collected at the right edge, with a similar match. Images from each case are also shown.

For the FA simulation in Figure 5, the same conditions and material parameters were used, except the dose was varied to achieve a very good match of the net effect of the basic imaging effects and charging. The waveform match has the yields almost exactly correct, and the shape of the edge is close, although the FA result has slightly more slope on the sidewall of the waveform than the MC result, which is the cause of the visually-observed differences in the edge, although this is considered to not be a large difference for this work since it should result in a systematic shift of the entire edge so amplitudes of the sidewall features should not be effected severely. A small foot can also be seen in the MC results which is absent in the FA result, and the FA results show a slight “charging bump” inside the edge, but neither the foot nor bump will be important to solving edge locations, as edges will be found with a simple threshold algorithm which will avoid those waveform discrepancies.

Thus, use of the FA method is a valid choice for a good quantitative estimation of charging effects while keeping the simulation times reasonable for the study. The FA method for image generation will thus be used for the remainder of

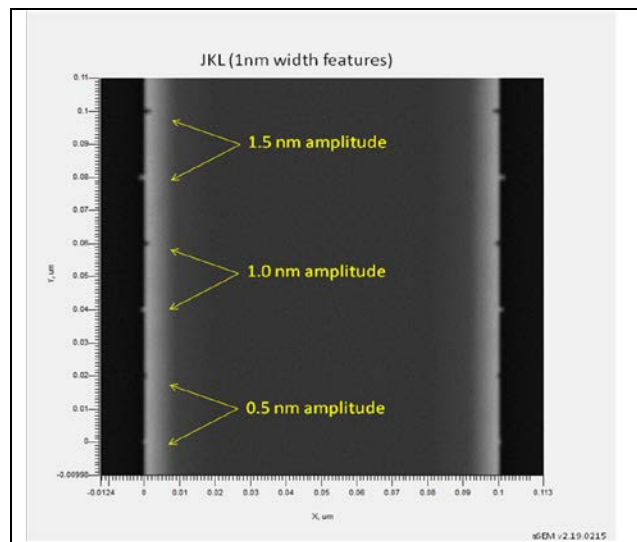


Figure 6: JKL sector of the sample DOE, including all the 1 nm wide tabs and inclusions with all three different designed amplitudes. This image was generated by aSEM using 1.2 nm FWHM 500 V Gaussian beam with 10 pA beam current and 0.0001 μ s integration time, charging turned off, and 0.25 nm pixels.

this work. An example image is shown in Figure 6. This and the entire family of non-charging and charging images over the entire DOE will be further analyzed in the next section.

ANALYSIS

After generating the images over the entire DOE with the FA simulations, the images were analyzed using MetroLER v1.8 software by Fractilia. This software allows edge detection with sub-pixel interpolation using a plethora of different edge algorithms, although to keep our study simple and not convolute the analysis with one model on top of images generated by another model, we will use the typical simple threshold algorithm, with threshold = 50%. Figure 7 shows an example output.

Once the edges are analyzed and output numerically, the average apparent location of the edge in regions away from these sidewall features is calculated as the baseline position of the edge, which serves as the reference for the tab and inclusion amplitudes. The edge is physically located at $x = 0$ nm and $x = 100$ nm, but due to the edge blur and interaction with the edge algorithm, the apparent edge will be close but slightly off from those values, but the same is true for the peaks and troughs of the edge at the tab/inclusion features, so those amplitudes are calculated with respect to that apparent average edge location, leading to edge deviation functions.

Figure 8 shows some example edge deviation functions for larger and smaller features. With the deviations, it was a simple task to extract the amplitudes of the peaks and troughs of the edges with maximum and minimum functions within the various spatial regions. In some cases where the sidewall features were wider with minimal curvature around the peak of the extrusions/intrusions, a few pixels at the peak were averaged as a lower noise alternative.

Once all the edges are analyzed for the feature amplitudes, the average linear response of the edge location changes due to the varied sidewall features can be evaluated as slopes (measured amplitude versus designed or actual amplitude). In these, since any nominal 0 nm feature will obviously give 0 nm amplitude response, the lines of best fit are constrained to always go through the origin.

Figure 9 shows examples of these sensitivities of the metrology to such known sample variations. The net effect of the results is shown in the bottom left graph, where features 1.5 nm wide and larger have a near unity response, whereas for smaller features, the response decreases rapidly. Note that the FWHM of the defined beam in these simulations was 1.2 nm.

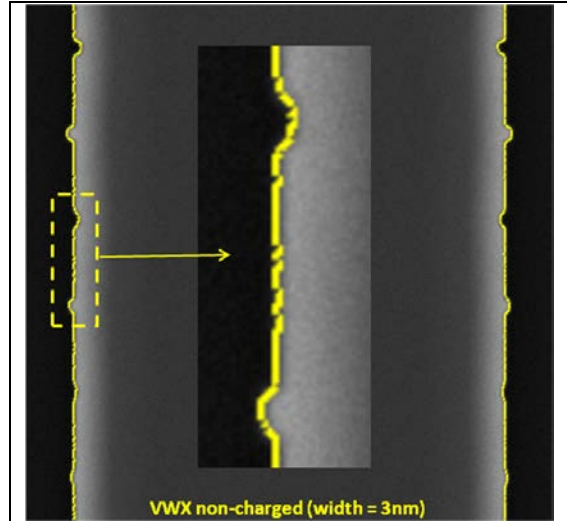


Figure 7: Example of edge detection results from the analysis using Fractilia's MetroLER software. The edges are available for numerical analysis.

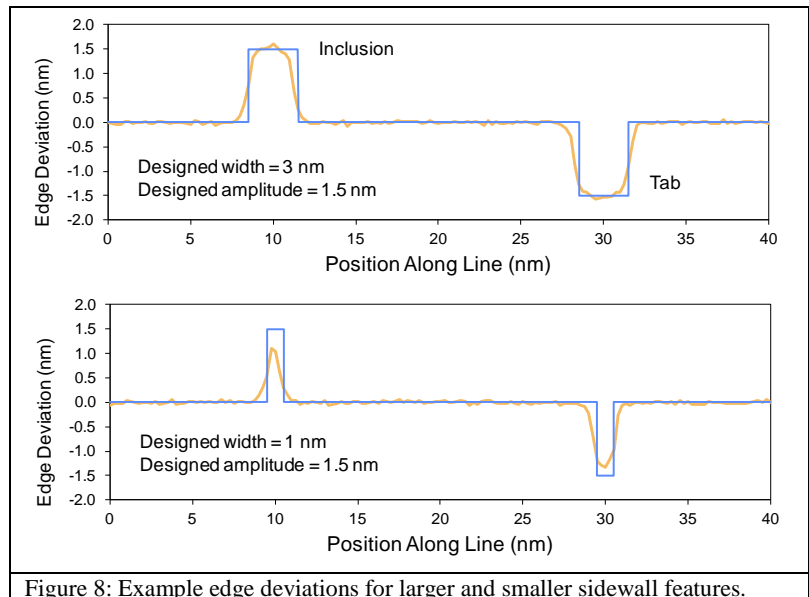


Figure 8: Example edge deviations for larger and smaller sidewall features.

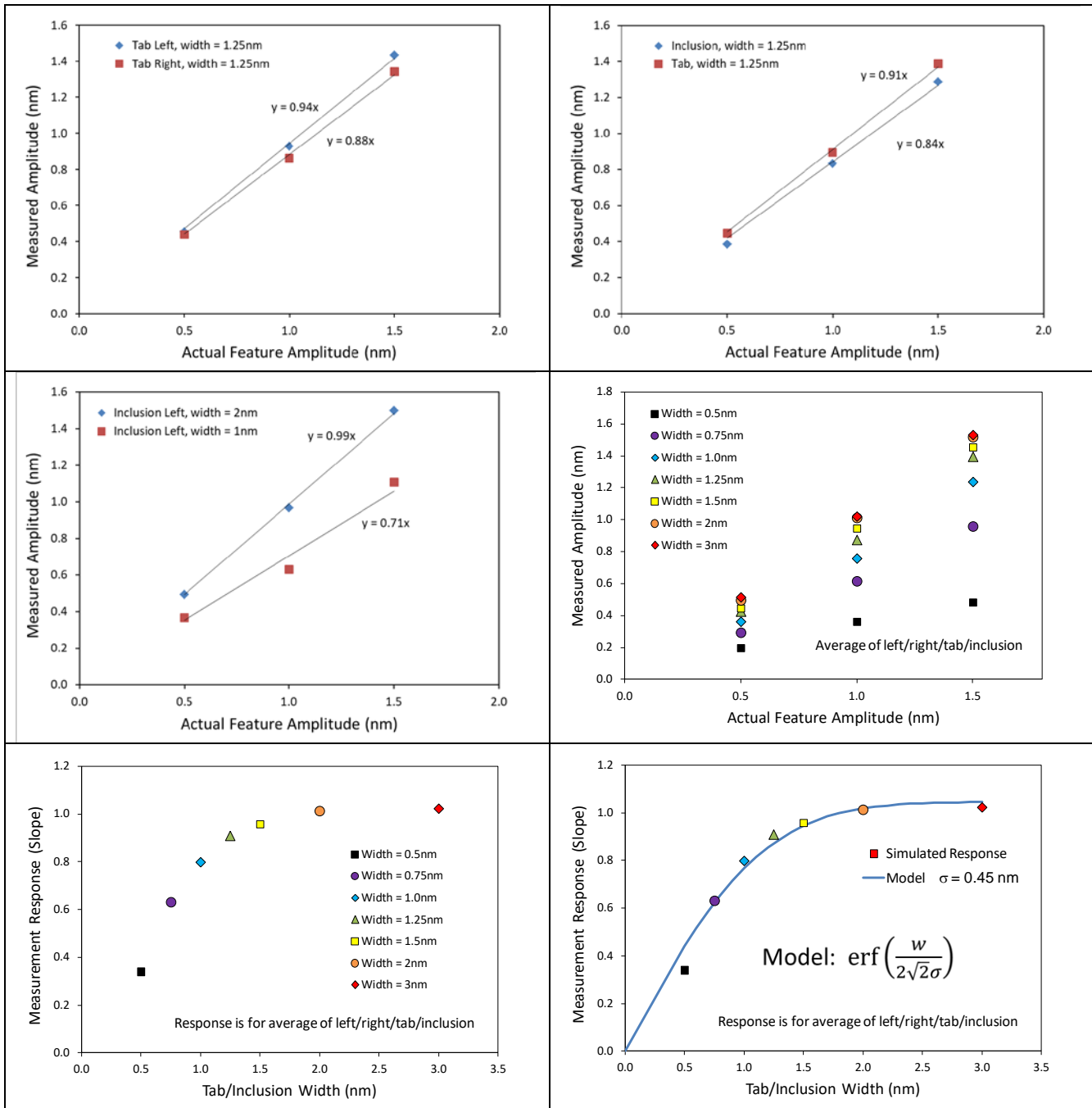


Figure 9: Example amplitude responses over the line, including charging effects, assuming scan direction convention is left-to-right. Top Left: 1.25 nm designed amplitude tabs on opposite sides of a charged line, showing a different response slope for the features. This means the image response is more sensitive to the tabs on the leading edge of the scan. Top Right: 1.25 nm designed amplitude tabs and inclusions on left side of a charged line, showing a different response slope for the features, meaning that on the leading edge of the scan the image response is more sensitive to tabs than inclusions. Middle Left: Comparison of metrology response in non-charging case, showing how much smaller slope becomes as the feature designed widths decrease, with the 1 nm wide feature having much less response (slope) than the 2 nm wide feature. Middle Right: Comparison of all non-charging results for the different feature sizes showing the trend for less metrology response for narrower features (narrower features are cooler colors, wider features as hotter colors). Bottom Left: Slopes from the Middle Right graph plotted by designed feature width and same legend. Bottom Right: Curve fit to solve for blur (σ) with the given responses and widths w . Blur was solved to be $\sigma = 0.45$ nm in this case.

As mentioned in the introduction to this work, we wish to analyze blur for these various cases, and the measurement responses in the bottom left graph of Figure 9 can be analyzed as an example. We assume the SEM-detected feature is a Gaussian convolved with the actual designed feature shape, thus the Gaussian with blur parameter σ is convolved with a rectangle (tab or inclusion) of width w . The peak response will thus be an error function:

$$\text{erf}\left(\frac{w}{2\sqrt{2}\sigma}\right)$$

The widths are known (simulation inputs) so with the evaluated responses, blur σ is solvable. In the next section we will show the final blur results, and compare these blurs among different subsets of considerations among the DOE.

RESULTS & DISCUSSION

Figure 10 shows the metrology responses for the case without charging. Curve fit solutions for blur σ and the σ values are also shown. The non-charging case is what is widely understood and is less interesting than when charging is included, but two observations can be made: the results are the same for either edge, and the tabs have slightly less blur than the inclusions, thus tabs will effectively be better resolved than the inclusions.

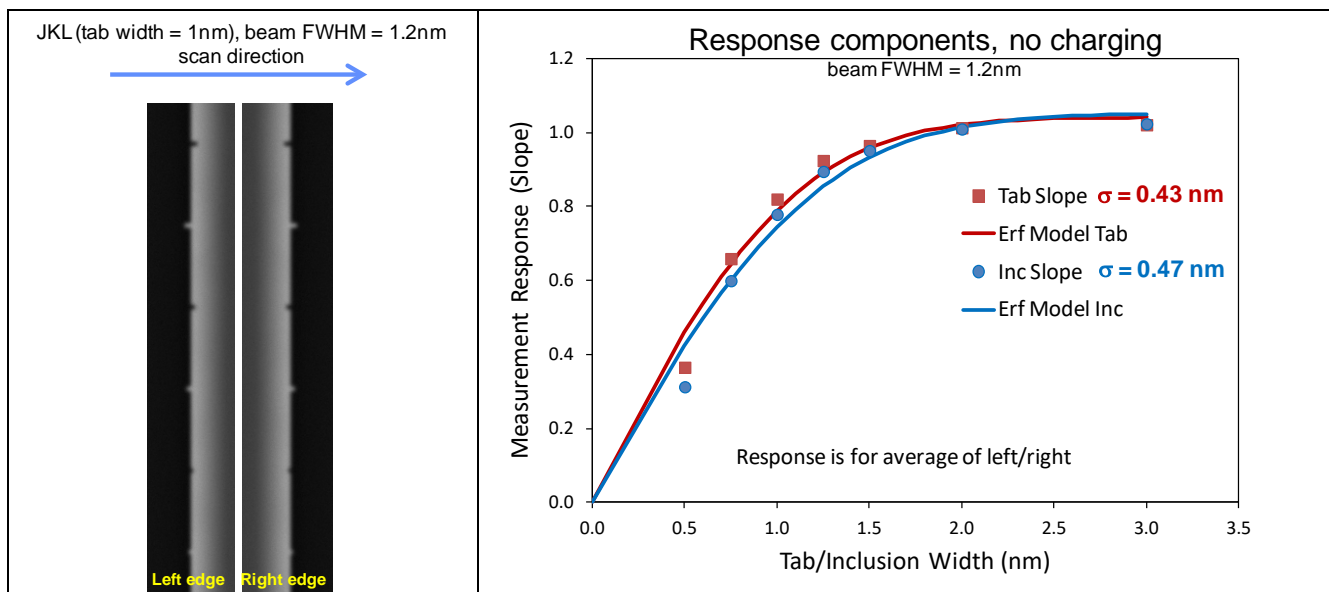


Figure 10: Metrology response results for the non-charging case. Left: Example images of both sides of line. Right: Response components for tabs and inclusions, with the model fits per the reported σ blur values. Blur values are color-coded same as corresponding feature type. Since in non-charging case the responses are symmetrical, the tabs' and inclusions' slope values are averages of results from both edges.

Figure 11 shows the metrology responses for the charging case, and here we can see the source of much asymmetry between opposite sides of the line. In these results, the left (leading) side tabs (extrusions) have less blur, or better effective resolution, than the same tabs on the right (trailing) side of the line. The inclusions behave similarly but in the opposite direction: the right (trailing) inclusions have much less blur than the left (leading inclusions) meaning that these trailing inclusions will have much better effective resolution, almost by a factor of two.

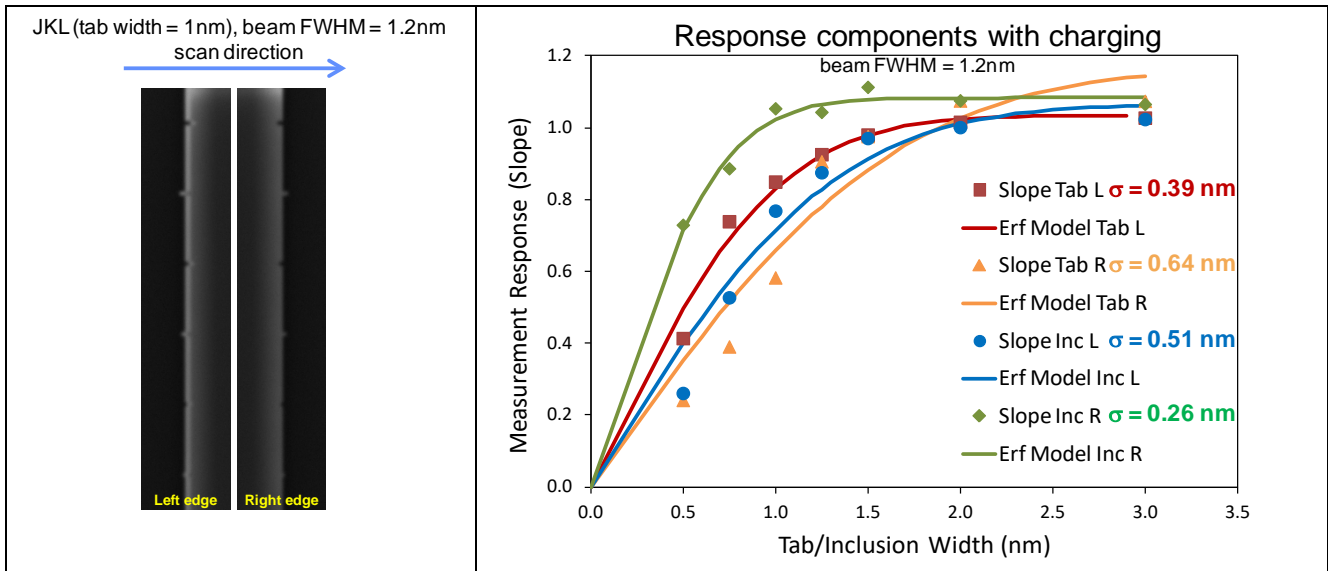


Figure 11: Metrology response results for case including charging. Left: Example images of both sides of line. Right: Response components for tabs and inclusions on both left and right sides of line (same as leading and trailing edge, respectively), with the model fits per the reported σ blur values. Blur values are color-coded same as corresponding feature type. Large difference in the imaging of the feature types appear here: left tab (red) has considerably less blur than the right tab (orange), while right inclusion (green) has almost half the blur of the left inclusion (blue).

The results in Figures 10 and 11 include multiple levels of feature subsets that can be independently evaluated for blur, so that different components can be compared. Additionally, the entire exercise was repeated for a second beam spot size with FWHM = 2.0 nm, i.e. 66% larger than the other beam while all other parameters and the DOE held constant, to see how such responses scale. Results of the components are shown in Figure 12.

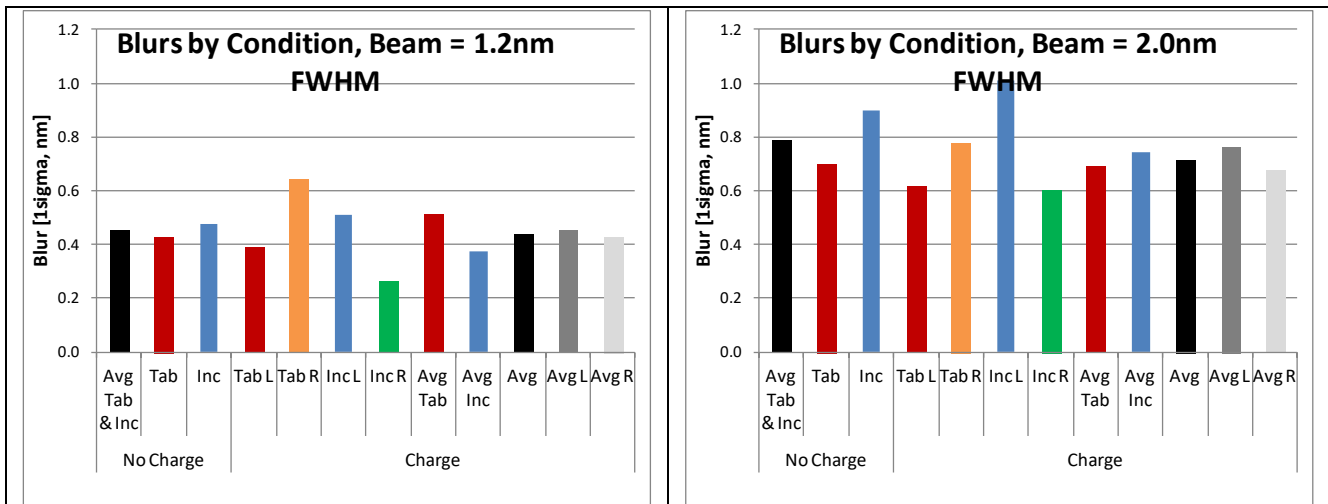


Figure 12: Blurs for different subsets of features from DOE for (left) 1.2 nm and (right) 2.0 nm FWHM spot sizes. Within each spot size, the non-charging case has values for all features combined (average of tabs and inclusions) then averages for tabs and for inclusions. The charging case has many more components, including tabs left and right, inclusions left and right, average of all tabs and average of all inclusions, and averages for all features on left and on right.

Note that the results shown for the 2 nm beam are mostly very proportional to those with the 1.2 nm beam, with the exception that inclusions have increased blur with respect to the tabs for the larger beam; this makes sense as the sizes of the features in the DOE did not also scale with the increase in spot size, so we expect the relative effects between the

tabs and inclusions to change. Other from that, the other trends act very repeatably and proportionally. Below in Figure 13, we point out the meaningful comparisons from Figure 12's 1.2 nm beam results.

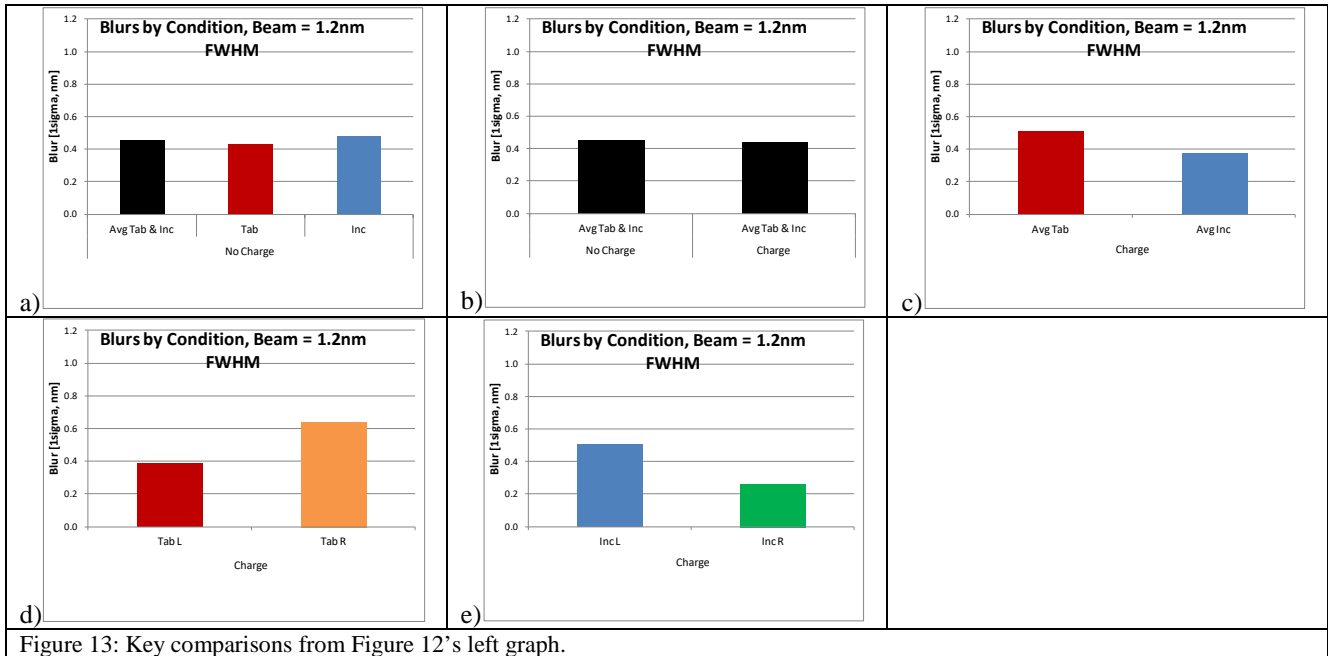


Figure 13: Key comparisons from Figure 12's left graph.

Figure 13a shows that tabs have slightly less blur than inclusions in the non-charging case, however this difference is minor. Figure 13b compares the average of all features in the non-charging case compared to the charging case, with the result being almost identical average blur—thus charging really does not add a net blur to the entire response, on average—it affects smaller subsets of sidewall features asymmetrically. Figure 13c compares averages of all tabs to all inclusions in the charging case, and with the 1.2 nm beam the inclusions have significantly less blur on average, while Figures 13d and 13e respectively show the almost 2x asymmetry of the blur for tabs and for inclusions, and how the asymmetries between them switch direction—tabs have less blur on leading edge of scan, and inclusions have less blur on trailing edge of scan.

CONCLUSIONS

In this work, Monte Carlo-validated Fast Analytical SEM image simulations of a sidewall feature DOE were measured for amplitude and analyzed for blur. We quantitatively demonstrated that charging does not add more blur. However, charging adds asymmetrical blur effects for different sidewall features, with different behaviors on leading and trailing edges of the line. Tabs image sharper on left (leading) edge of the scan, and inclusions image sharper on right (trailing) edge of the scan, assuming scan direction is left-to-right.

As shown earlier in Figure 2, SEM blur depresses high frequency PSD. Thus charging adds another component towards decreasing the high frequency PSD, and does this asymmetrically between the opposite sidewalls. And as shown in Figure 3, such extra blurring also means the PSD roll-off exponent metric will increase with charging, and thus be overestimated with respect to reality. Also as a ramification, the integral under the PSD is decreased (though the effect is slight).

REFERENCES

- [1] S. Babin, S. Borisov, A. Ivanchikov and I. Ruzavin. "CHARIOT: Software tool for modeling SEM signal and e-beam lithography", *Physics Procedia*, Volume 1, Issue 1, August 2008, Pages 305-313 (2008), <https://doi.org/10.1016/j.phpro.2008.07.110>.
- [2] S. Babin and S. Borisov. "Simulation of scanning electron microscope images taking into account local and global electromagnetic fields", *Journal of Vacuum Science & Technology*, **B28**, C6C41 (2010); <https://doi.org/10.1116/1.3518917>.
- [3] Benjamin D. Bunday and Chris A. Mack, "Influence of Metrology Error in Measurement of Line Edge Roughness Power Spectral Density", *Metrology, Inspection, and Process Control for Microlithography XXVIII, Proc.*, SPIE Vol. 9050, p. 90500G (2014).
- [4] Chris A. Mack and Benjamin D. Bunday, "Analytical Linescan Model for SEM Metrology", *Metrology, Inspection, and Process Control for Microlithography XXIX, Proc.*, SPIE Vol. 9424, p. 94240F (2015).
- [5] Chris A. Mack and Benjamin D. Bunday, "Improvements to the Analytical Linescan Model for SEM Metrology", *Metrology, Inspection, and Process Control for Microlithography XXX, Proc.*, SPIE Vol. 9778, (2016).
- [6] Chris A. Mack and Benjamin D. Bunday, "Using the Analytical Linescan Model for SEM Metrology", *Metrology, Inspection, and Process Control for Microlithography XXXI, Proc.*, SPIE Vol. 10145 (2017) p. 101451R.
- [7] Chris A. Mack and Benjamin D. Bunday, "CD-SEM Algorithm Optimization for Line Roughness Metrology", *Metrology, Inspection, and Process Control for Microlithography XXXII, Proc.*, SPIE Vol. 10585 (2018) p. 105850G.
- [8] Chris A. Mack, "Systematic Errors in the Measurement of Power Spectral Density", *Journal of Micro/Nanolithography, MEMS, and MOEMS*, Vol. 12, No. 3 (Jul-Sep, 2013) p. 033016.
- [9] S. Babin, S. S. Borisov and V. P. Trifonenkov. "Fast analytical modeling of SEM images at a high level of accuracy", *Metrology, Inspection, and Process Control for Microlithography XXIX, Proc.*, SPIE Vol. 9424 (2015) p. 94240I.
- [10] S. Babin, S. Borisov, N. Khmelevsky and V. Trifonenkov. "Comparison of SEM image simulation results using fast analytical modeling and Monte Carlo", *Metrology, Inspection, and Process Control for Microlithography XXXII*, poster, available upon request (2018).